Environmental Modelling and Software 158 (2022) 105543

Contents lists available at ScienceDirect

Environmental Modelling and Software

journal homepage: www.elsevier.com/locate/envsoft

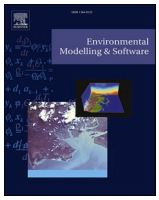

Investigation of effect of logjam series for varying channel and barrier physical properties using a sparse input data 1D network model

Elizabeth Follett [a,*], Barry Hankin [b,c]

[a] Hydro-environmental Research Centre, School of Engineering, Cardiff University, Cardiff, Wales, UK
[b] Lancaster Environment Centre, Lancaster University, Lancaster, UK
[c] JBA Consulting, 1 Broughton Park, Broughton, Skipton, North Yorkshire, BD23 3FD, UK

ARTICLE INFO

Keywords:
Engineered logjam
R
Flood hydraulics
Backwater
Nature-based solutions
Hydraulic model

ABSTRACT

Targeted design and placement of natural flood management leaky barriers, or engineered logjams, and accurate representation of logjams in hydraulic models across different scales is necessary to generate desired water storage and flood peak attenuation for effective river restoration and natural flood management projects. We systematically assess the effect of varying logjam spacing, extent of logjam-generated change in water surface profile, vertical height of lower gap, overflow to local floodplain, and varying channel slope, representing a series of logjams in a sparse input data 1D network model including the jam-generated backwater, which depends on loss of momentum within the jam. To guide catchment-scale representation, best-fit increased channel resistance was found to increase with number of jams, approaching an analytically determined maximum for close inter-jam spacing, useful for setting an upper envelope for efficacy.

1. Introduction

The presence of large wood [LW, defined as logs with diameter ≥ 0.1 m and length ≥ 0.1 m] (Keller and Swanson 1979; Wohl and Jaeger 2009), in river channels increases flow heterogeneity and habitat diversity. Engineered logjams composed of many smaller wood pieces are installed as part of river restoration and natural flood management projects to provide the physical and ecological benefits associated with LW (Gallisdorfer et al., 2014; Bennett et al., 2015; Burgess-Gamble et al., 2018; Dadson et al., 2017; Ismail et al., 2021). However, knowledge gaps surrounding the effectiveness of natural flood management interventions and the physical processes by which jams affect channel-floodplain connectivity and water storage have led to calls for evidence (Wohl et al., 2016; Dadson et al., 2017; Burgess-Gamble et al., 2018) and process-based investigation (Wohl et al., 2005) to improve the design and assessment of interventions using LW.

Logjams create an upstream area of slower, deepened water, increasing habitat diversity and potential for deposition of sediment and fine particles (Bilby, 1981; Bouwes et al., 2018; Schalko et al., 2018). The increase in upstream water depth, or backwater rise, generated by logjams (Geertsema et al., 2020) has recently been described with momentum-based models, with drag generated by the group of logs in the jam region represented by an adaptation of the law for drag in canopies (Follett et al., 2020, 2021). This approach allows representation of logjams as hydraulic structures in a flood model or network analysis (Ruíz Villanueva et al., 2014, Metcalfe et al., 2017; Persi et al., 2019; Hankin et al., 2020; Leakey et al., 2020; Senior et al., 2022). However, a research gap remains in predictive approaches for large catchments, for which representation of tens to hundreds of jams may be desired. At this scale, individual jam representation is time-intensive and can require mesh refinement and associated timestep reduction to maintain the Courant-Friedrichs-Lewy (CFL) condition ($u\Delta t \ll \Delta x$), increasing model runtime. Previous investigators have represented the aggregate effect of multiple logjams with an empirically determined increase in channel hydraulic roughness (Addy and Wilkinson, 2019). In addition to LW implementation, uncertainty in flow measurement and boundary conditions can complicate prediction of natural flood management (NFM) schemes. These uncertainties can be made more explicit using, for example, the General Likelihood Uncertainty Estimation (GLUE) framework (Beven and Binley, 1992a, 1992b), and the influence of NFM in general can be investigated in a more complex uncertainty framework (Hankin et al., 2017) whereby stratified sampling is undertaken of the uncertainties in both the controlling parameter and the expected perturbation to it due to NFM. Field observations of engineered

* Corresponding author.
E-mail address: emf@alum.mit.edu (E. Follett).

https://doi.org/10.1016/j.envsoft.2022.105543
Received 6 July 2022; Received in revised form 28 September 2022; Accepted 2 October 2022
Available online 7 October 2022

and natural LW jams (Black et al., 2020; Linstead and Gurnell 1999) have observed that the effect of jams is expected to depend on both channel and barrier physical properties, calling for additional research investigating the comparative effects across river channel and barrier physical parameters.

In this paper we explore the effect of a series of jams on a varying inflow hydrograph for varying magnitude of jam longitudinal density, jam-generated backwater rise, lower gap height, local overflow to surrounding floodplain, and channel physical properties to demonstrate the effect of varying jam properties and guide choice of jam design for varying channels. To guide choice of effective channel resistance based on barrier physical properties for large spatial scale modelling approaches, we choose an effective bed friction coefficient C_{fe} yielding minimum sum of the squared difference in volume between outflow exiting 1D networks representing reaches of length L_R containing multiple logjams, and the same model channel with effective resistance represented by C_{fe}, instead of individual jams. Model jams had accumulation factor C_A and average inter-jam spacing L_s. The backwater rise upstream of each jam depends on the jam accumulation factor and unit discharge (Follett et al., 2020, 2021). The effect of predicted C_{fe} on channel outflow discharge downstream of eight leaky barriers is demonstrated and compared to implementation of individual barriers as hydraulic structures in HEC-RAS 2D, representing Penny Gill, West Cumbria, UK [Fig. 1(a)].

2. Theory

2.1. Unobstructed open channel flow

The effect of a series of jams on outflow discharge and channel segment water volume was compared to the effect of uniform flow with constant bed resistance in a wide rectangular open channel of reach length L_R, slope S, width B, bankfull depth H_{bf}, and gravitational acceleration g. Uniform flow depth h_0 resulted from a balance between the weight of water on bed slope S balanced by bed friction, represented by a dimensionless bed friction coefficient C_{f0} (Julien 1998, 2010).

$$Q = B\left(\frac{gh_0^3 S}{C_{f0}}\right)^{1/2} \tag{1}$$

The bed friction coefficient C_{f0} can be related to the Chézy coefficient, $C_{f0} = 1/C_z^2$, and Manning's resistance coefficient in a wide channel $C_{f0} = n_0^2 g/h_0^{1/3}$ (Julien 1998, 2010). The bed friction coefficient was related to bankfull depth and median bed sediment diameter D_{s50}

$$C_{f0} = \left[5.75\, log_{10}\left(\frac{2H_{bf}}{D_{s50}}\right)\right]^{-2}, \tag{2}$$

assuming a logarithmic profile for mean longitudinal velocity (Julien 1998, 2010). In this paper C_{f0} and uniform flow were predicted from measured H_{bf}, B_{bf} and D_{s50} using observations of UK rivers (Hey and Thorne, 1986). In general, the mean sediment diameter and bankfull channel depth increase with increasing slope. For channels where median sediment diameter is not known, an estimation of bed resistance based on channel slope was used to reduce amount of input data. For channels with $S \geq 0.015$, bed resistance may be estimated from the relationship found by Yochum et al. (2014) from field observations of high gradient streams ($n = 1.85S^{0.79}, S = 0.015 - 0.21$). For a channel with unknown median sediment diameter and $S < 0.01$, C_{f0} may be related to channel slope using the regression relationships of Parker et al. (2007) for H_{bf}

$$H_{bf} = \frac{0.382}{g^{1/5}} Q_{bf}^{2/5} \tag{3}$$

and D_{s50},

$$D_{s50} = \left[\frac{Q_{bf}}{\sqrt{g}}\left(\frac{0.101}{S}\right)^{-2.91}\right]^{2/5} \tag{4}$$

so that

$$C_{f0} = \left[5.75\, log_{10}\left(\frac{0.0535}{S^{1.16}}\right)\right]^{-2}, \tag{5}$$

allowing prediction of C_{f0} and Q for channels with a given slope and bankfull width. To estimate uniform flow, C_{f0} is first found from S using Eq. (5), enabling solution of H_{bf} from measured B_{bf} and Eqs. (1) and (3) and prediction of Q using Eq. (1). UK rivers were observed to be relatively deeper and narrower compared to the full dataset used by Parker et al. (2007), which was attributed to the high density of bank vegetation and lower expected gravel supply relative to other sites used (Alberta, Canada, and Idaho and Colorado, USA). In addition, bankfull width varied more strongly with discharge than bankfull depth across the full dataset (Parker et al., 2007). Therefore, use of both measured H_{bf} andB_{bf} is preferable, but if necessary prediction of H_{bf} is preferred over bankfull width as the magnitude of error in the prediction is less severe. While local observations of H_{bf}, B_{bf} and D_{s50} may differ from the predictions of Eqs. (3) and (4) due to local channel adjustment and sediment input, prediction of D_{s50} and C_{f0} from channel slope and bankfull width is suitable for use in sparse data input methods where H_{bf} and D_{s50} are not available.

2.2. Jam-generated upstream backwater rise

Flow through a jam generated momentum loss proportional to the number, size, and packing density of the logs comprising the jam (Follett et al., 2020, 2021), elevating the water depth upstream of the jam h_J relative to unobstructed open channel flow. Flow through a jam with a lower gap was a combination of unit discharge $q = Q/B$ passing through

Fig. 1. (a) Engineered logjam installed in Penny Gill, West Cumbria, UK. (b) Photo of channel-spanning jam installed in Nant Drysiog, Bryn, UK, with upstream water depth above the jam top edge, generating local floodplain inundation. Photo recorded during Storm Dudley (February 16, 2020).

the jam and lower gap sections:

$$q = \left[\frac{2g(h_J - a)^3}{3\sqrt{3}\,C_A}\right]^{1/2} + \left[\frac{C_{p0}}{\left(1 + C_b\frac{a}{h_J}\right)} g a^2 h_J\right]^{1/2} \quad (6)$$

with vertical width of the lower gap a, dimensionless jam structural parameter C_A related to the jam length L_J, drag coefficient for a rigid circular cylinder $C_d \cong 1$, frontal area density a_f, and solid volume fraction φ ($C_A = L_J C_d a_f/(1-\varphi)^3$; Follett et al., 2020), gate discharge coefficient $C_{p0} = 2/3$ and $C_b = \frac{C_{p0}C_f}{S} - 1$ (Malcherek 2018; Follett et al., 2021). C_A increases with the amount of solid wood present in the jam, and extent of jam-generated change in water surface profile increases with increasing C_A. Equation (6) corresponds to the upstream depth for a channel-spanning jam (Follett et al., 2020) when the lower gap vertical width $a = 0$,

$$q = \left[\frac{2g(h_J)^3}{3\sqrt{3}C_A}\right]^{1/2} \quad (7)$$

To link the jam structural parameter to readily obtainable field observations, C_A was related to the relative magnitude of jam-generated backwater rise. The upstream backwater depth generated by a channel-spanning jam [Eq. (7)] was compared to unobstructed uniform flow in a wide channel [Eq. (1)], for the same unit discharge,

$$C_A = \frac{2}{3\sqrt{3}} * \frac{C_{f0}}{S(h_0/h_J)^3} \quad (8)$$

with the relationship between C_A and relative ratio h_0/h_J independent of unit discharge for a channel-spanning jam in a wide channel, due to correspondence between Eq. (1) and Eq. (7). For a channel of increasing slope, a lower C_A (less wood pieces in jam) would be required to generate a given relative h_0/h_J, compared to a lower slope channel. To compare the effect of varying C_A in a consistent manner across channels of varying slope, low, medium, and high density jams were defined by relative ratio $h_0/h_J = 0.25, 0.33, 0.5, 0.75$ with the uniform flow depth equal to h_0/h_J times the jam-generated upstream backwater depth. A ratio of $h_0/h_J = 1$ would indicate an unobstructed channel. The backwater volume generated by flow passing through a jam was found from uniform flow and jam-generated upstream flow depths [Eqs. (1) and (6)].

2.3. Jam submergence and local floodplain inundation

At water depths higher than the elevation of the jam top edge, flow has been observed to pass over the top edge of the jam and inundate the local floodplain (Fig. 1). Discharge passing over the jam top edge H_J was represented by a sharp-crested weir (Hankin et al., 2020),

$$Q = B\frac{2}{3}\sqrt{2g}(h_J - H_J)^{3/2} + Q(h_J = H_J) \quad (9)$$

with discharge when upstream water depth is equal to the height of the jam top edge above the bed $Q(h_J = H_J)$ given by Eq. (6). For correspondence with previous work identifying floodplain roughness coefficients (Chow 1959, Yochum et al., 2014), floodplain roughness was represented by Manning's coefficient, n_0 (s m$^{-1/3}$) with uniform flow depth given by Manning's law, instead of the dimensionless friction coefficient model used to describe bed resistance in the channel:

$$Q = \frac{B^{5/3}h_0^{5/3}\sqrt{S}}{(B + 2h_0)^{2/3}n_0}. \quad (10)$$

Two methods were used to explore the effect of jam-generated inundation of a simplified local floodplain. For jams with elevation of top vertical edge above the bed H_J less than or equal to the channel bankfull depth, discharge passing over the top edge of the jam was represented by Eq. (9) and floodplain resistance was represented by Eq. (10). Local floodplain width was assumed to be equal to the channel bankfull width on either side of the channel, so that total width of the channel and floodplain was three times the channel bankfull width. The simplified floodplain geometry and width were intended to estimate the effect of overtopping and local inundation. In future work, the choice of width and geometry should be clarified with reference to empirical observations. For jams with height of top vertical edge greater than the channel bankfull depth, flow was assumed to occupy a total width of three times the channel bankfull width, passing through a channel spanning jam [Eq. (7)] with equivalent C_A to the in-channel jam. In this method the jam-generated momentum loss was assumed to be much greater than the floodplain resistance, so that the contribution of floodplain resistance was neglected. Water depth above the jam top edge was represented by a weir [Eq. (9)].

2.4. Volume of jam-generated upstream backwater

The network model used in this paper related the unobstructed, uniform and jam-generated upstream water depths to total volume of water in a channel segment (Hankin et al., 2020). Water volume in a channel segment containing a jam at the segment downstream edge was assumed to occupy a combination of uniform flow and a simplified, triangular upstream backwater region (Fig. 2). This assumption is a simplification of the true backwater curve, which asymptotically approaches uniform flow depth (Chow, 1959). A region of falling water at the downstream face of the jam and contracted flow exiting the jam were observed under some experimental conditions (Follett et al., 2021). The channel was assumed to have $S < 0.17$, so that error introduced by the small angle approximation $\tan(\theta) = \sin(\theta) = \theta$ was less than 1%. The jam generated an upstream water depth h_J (Fig. 2, blue solid line), with backwater length extending from the jam upstream edge over a distance $L_{bw} = (h_J - h_0)/S$ until the absolute elevation of the channel water surface at uniform flow was equal to the water surface elevation upstream of the jam. Total jam length L_J was assumed to be much smaller than L_{bw}, so that in-jam water storage was neglected. The volume of water in a segment with maximum water depth $h_J < H_{bf}$ and $L_{bw} < L_s$ was then

$$V_s = V_{bw} + V_0 = BL_s h_0 + B\frac{1}{2}L_{bw}(h_J - h_0) \quad (10)$$

Effective channel width increased for water depths above H_{bf}. For a channel segment with $h_J > H_{bf}$, the volume of water above the local floodplain,

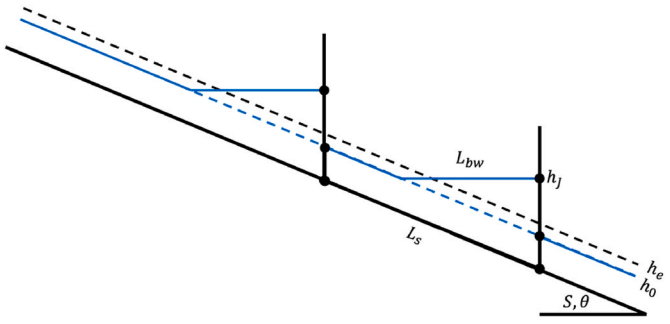

Fig. 2. Schematic diagram of simplified jam-generated upstream backwater. Backwater rise $h_J - h_0$ generated by jam with inter-jam spacing L_s in a channel with unobstructed uniform water depth h_0. The modification of outflow discharge due to a series of jams was represented by an effective water depth, h_e, which is related to unit discharge with an effective resistance coefficient C_{fe}. The channel was assumed to have $S < 0.17$, so that error introduced by the small angle approximation $tan(\theta) = sin(\theta) = \theta$ was less than 1%. Channel slope exaggerated on figure to show full backwater on page.

$$V_{fp} = B\left(B_{eff} - 1\right)L_s h_{fp,0} + B\left(B_{eff} - 1\right)\frac{1}{2}\frac{\left(\Delta h_{fp,J}\right)^2}{S} \tag{11}$$

was added to the volume of water in and directly above the channel [Eq. (10)], with effective floodplain width assumed to be $B_{eff} = 3$ times the bankfull channel width. For cases with $h_J > H_{bf}$, the uniform water depth on the floodplain $h_{fp,0} = \max(0, h_0 - H_{bf})$ and the difference between the jam-generated flow depth on the floodplain and floodplain bed level or above-bankfull unobstructed flow depth $\Delta h_{fp,J} = \min\left(h_J - H_{bf},\ h_J - h_0\right)$. For segments with $L_{bw} > L_s$, the backwater volume within the channel segment was found from the difference between the total backwater volume in a long segment and the excess backwater volume beyond $x = L_s$ upstream of the jam.

The relative ratio of backwater volume to volume of unobstructed uniform flow V_{bw}/V_0 was used to guide a parameter study investigating the effect of a series of jams with varying channel and jam parameters at channel sites with varying slope. For a channel of width B containing a channel-spanning jam [Eq. (7)], V_{bw}/V_0 is then,

$$\frac{V_{bw}}{V_o} = \frac{1}{2}\frac{L_{bw}}{L_s}\left(\sqrt{3}\left(\frac{C_A S}{2C_{f0}}\right)^{1/3} - 1\right) \tag{12}$$

with the ratio of jam-generated backwater volume to volume of unobstructed uniform flow dependent on the ratio of backwater length to segment length L_{bw}/L_s, which increases with jam density along the reach, and $\frac{h_J}{h_0} \sim \left(\frac{C_A S}{C_{f0}}\right)^{\frac{1}{3}}$, which increases with C_A and increasing slope. A jam with a given C_A results in higher V_{bw}/V_0 at bankfull discharge in channels with increasing slope [Fig. 3(a)], but lower backwater length. Jams with higher C_A (lower h_0/h_J) generated higher relative backwater volume that increased more steeply with Q/Q_{bf} [Fig. 3(b)], consistent across varying channel sites.

3. Methods

3.1. Model channel properties

To guide choice of barrier design for varying channel properties, model runs were conducted for three UK rivers with $B < 10$ m and increasingly steep slope measured by Hey and Thorne (1986): the Chittern at Codford, Usway Burn at Shillmoor, and Burbage Brook at Burbage. Channel slope, bankfull width, bankfull depth, and median sediment diameter are given in Table 1. Investigation of jam density, varying C_A, gap height, and local floodplain overflow were run for the intermediate slope site Usway Burn at Shillmoor, while investigation of varying slope used the additional two sites. Discussion of model implementation of an effective resistance coefficient, as compared to a series of individual jams, used Penny Gill, West Cumbria, UK (Table 1; Hankin et al., 2020). Median sediment diameter was not measured for Penny Gill, and an effective Manning's bed resistance coefficient of $n_0 = 0.23$ was chosen based on the installation of scattered logs in the channel intended to elevate bed resistance (Yochum et al., 2014) in addition to a series of eight channel-spanning jams in the main channel and smaller barriers constructed upstream of the monitored reach.

Table 1
Channel parameters S, B, H_{bf}, D_{s50} for the Chittern at Codford, Usway Burn at Shillmoor, and Burbage Brook at Burbage (Hey and Thorne, 1986) and Penny Gill (Hankin et al., 2020). Median sediment diameter was not measured for Penny Gill.

Site name	S (m)	B (m)	H_{bf} (m)	D_{s50} (m)
Chittern at Codford	0.001935	6.5	0.68	0.0232
Usway Burn at Shillmoor	0.008479	9.1	0.78	0.1135
Burbage Brook at Burbage	0.021467	5.5	0.72	0.1096
Penny Gill, West Cumbria	0.005	5	1	–

3.2. Network model

To systematically investigate the effect of longitudinal jam density, varying C_A, gap height, local floodplain overflow and correspondence to a best-fit effective elevated bed resistance model, a rectangular open channel containing a series of jams was represented by a 1D network, similar to previous frameworks used to assess assessing jam placement and network structure (Hankin et al., 2020). Model files were implemented in the R language. The network contained N_s nodes representing a series of channel segments. Each node i represented one channel segment with slope S_i, length L_i, average width B_i, and water volume V_i. The change in water volume within each segment was equal to the difference between inflow and outflow,

$$\frac{\partial V}{\partial t} = \sum_{j=1}^{N_s}\left(a_{ji}Q_j - Q_i + q_i\right), \tag{13}$$

with inflow Q_j entering segment i from the immediate upstream node j, and outflow exiting the segment downstream edge Q_i. Lateral inflow to

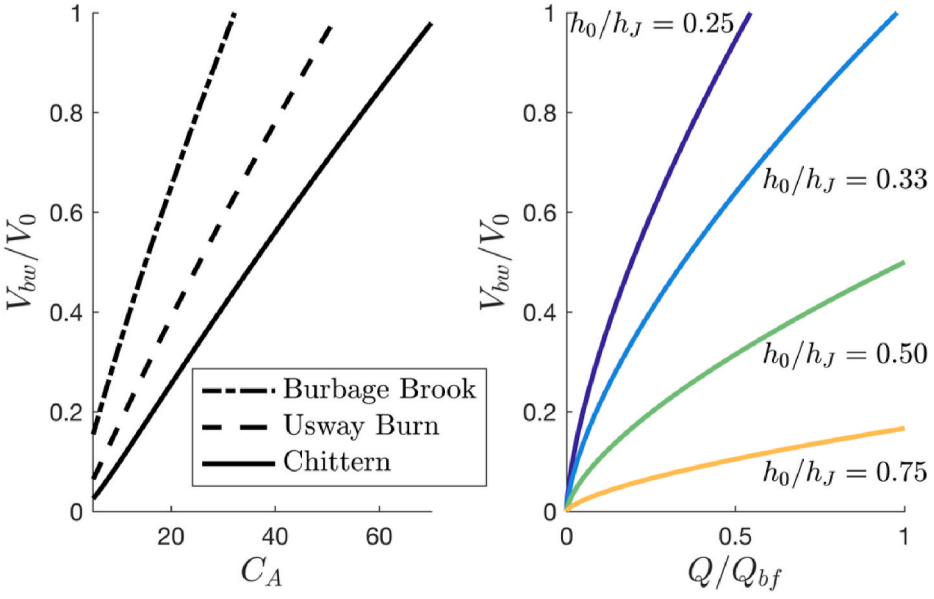

Fig. 3. (a) Jam-generated backwater volume above uniform flow depth relative to volume in a channel segment with uniform flow V_{bw}/V_0 for increasing C_A for the Chittern at Codford ($S = 0.001935$, solid black line), Usway Burn at Shillmoor ($S = 0.008479$, dashed black line), and Burbage Brook at Burbage ($S = 0.021467$, dash-dot black line), which had progressively increasing slope. Channel S, B, H_{bf}, D_{s50} given in Table 1. (b) Backwater volume above uniform flow depth relative to volume of uniform flow with increasing discharge relative to bankfull discharge Q/Q_{bf} for decreasing C_A, generating relative uniform flow depth to jam-generated upstream backwater depth $(h_0/h_J = 0.25, 0.33, 0.5, 0.75)$. Trend consistent across channels for the same relative h_0/h_J, Q/Q_{bf}.

segment i, q_i, is allowed in the scheme, although lateral inflow was not explored in this paper. Links between segments were represented with an adjacency matrix a_{ji}, with connection between node i and its immediate downstream neighbor j specified by $a_{ji}(i,j) = 1$ and $a_{ji}(i,j) = 0$ if no connection was present.

Values of discharge, segment water volume, and segment average cross-sectional area $A_i = V_i/L_{s,i}$ for each segment were interpolated from a precalculated hydraulic table. To generate the table, a range of possible node upstream water depths $h_J = (0-10)H_{bf}$ was specified. For nodes with no jam present, the upstream node depth was equal to the uniform flow depth throughout the segment. Discharge corresponding to uniform flow depth was found from Eq. (1), and segment volume and cross-sectional area for uniform flow were found by assuming a constant water depth h_0 along the reach [V_0, V_{fp0} in Eqs. (10) and (11)]. Discharge corresponding to node upstream depth for segments with a jam present was found from Eq. (6). For segments in which the upstream backwater did not occupy the full segment length, water depth upstream of the backwater was assumed to have uniform flow depth. The corresponding total segment water volume from backwater and uniform flow was found from Eqs. 10 and 11. The nonlinear system of equations describing conservation of mass [Eq. (13)], together with calculated $Q(g, h_0, S, C_{f0}, h_J, a, C_A)$ and $V(L_s, B, h_0, h_J, S, B_{eff}, H_{bf})$ found from Eqs. (1), (6), (10) and (11), describes the temporal evolution of node upstream water depths h_i. The equations are forced by source terms q_i, and each equation is coupled with equations corresponding to the upstream edge of the network. The system is solved numerically using an ordinary differential equation solver in R (lsodes). Code has been published in the GitHub repository. Although several hydraulic modelling software packages are available to solve similar equation sets, implementation of this system in a simplified 1D framework and open-source R language allows rapid implementation of many jams along a channel and assessment of a range of channel and barrier physical properties. In addition, this modelling framework provides a basis for future testing of arbitrary networks (Hankin et al., 2020).

4. Results

4.1. Number of jams per reach length

The effect of jam longitudinal density along the reach length, which increased L_{bw}/L_s [Eq. (12)], was explored by comparing the outflow from reaches containing successive numbers of jams. Channel properties corresponded to the Usway Burn at Shillmoor (Table 1) with total reach length $L_R = 27610$ m including a 10 m segment downstream of the last jam at which uniform flow depth was evaluated. An infinitely deep channel and jams were chosen to isolate the effect of varying jam longitudinal density, with maximum inflow found from the expected bankfull discharge for the site. Relative maximum backwater length varied from $L_{bw,max}/L_s = 0, 0.1, 0.25, 0.5, 1, 1.25, 1.5, 2, 2.92$ for $N = 0$, $10, 25, 50, 100, 125, 150, 200, 292$ jams. The jam accumulation factor $C_A = 68$ generated a relative ratio between uniform flow depth and jam-generated upstream depth $h_0/h_J = 0.25$. Discharge entering the reach was given by a Gaussian curve with maximum $Q = Q_{bf} = 11.83$ m^3/s, minimum base flow discharge $Q = 0.2Q_{bf}$, peak inflow discharge at $\mu =$ 6 h and variance of $\sigma = 1$ h [Fig. 4(a), solid black line]. The backwater tip reached the segment upstream edge at $Q/Q_{bf} = 0.72, 0.54, 0.35, 0.2$ for cases with $L_{bw,max}/L_s = 1.25, 1.5, 2, 2.92$. Spacing value $L_{bw,max}/L_s = 2.92$ was chosen so that $L_{bw,\max} = L_s$ at the minimum inflow discharge $Q = 0.2Q_{bf}$.

The jam-generated backwater has a greater increase in volume $\partial V/\partial$

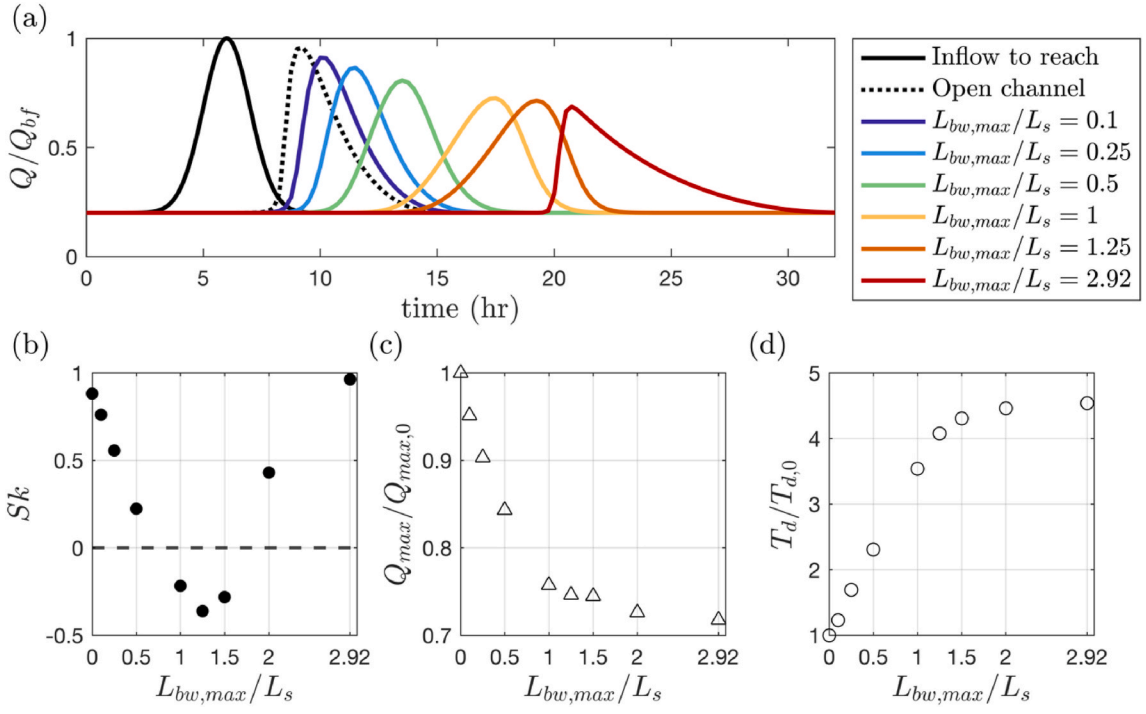

Fig. 4. (a) Discharge entering model reach (solid black line) and outflow discharge exiting reach relative to bankfull discharge with time (hr). Outflow from channels with successively increasing jam longitudinal density $L_{bw,max}/L_s = 0, 0.1, 0.25, 0.5, 1, 1.25, 2.92$ ($N = 0, 10, 25, 50, 100, 125, 292$ jams) for reach length $L_R = 27610$ with jams spaced over 27600 m represented respectively by solid dark blue, light blue, blue-green, green, yellow, orange, and red curves. (b) Skewness of residence time distribution of outflow discharge curve values above minimum base flow $Q = 0.2Q_{bf}$ with $L_{bw,max}/L_s$ for an unobstructed channel $T_{d,0}$ with $L_{bw,max}/L_s$ and $N = 0, 10, 25, 50, 100, 125, 150, 200, 292$ jams. Neutral skewness ($Sk = 0$) corresponding to a symmetric distribution indicated by horizontal black dashed line. (c) Relative magnitude of maximum outflow discharge compared to maximum outflow discharge from an unobstructed channel $Q_{max}/Q_{max,0}$ with $L_{bw,max}/L_s$ for cases in (b). (d) Time delay between peak inflow and outflow discharge for a channel with a series of jams T_d, relative to time delay for an unobstructed channel for cases in (b).

Q at higher discharge levels, as the backwater extends further upstream with increasing $h_J - h_0$ (Fig. 2). Consistent with the expected increase in relative impact of jam backwater volume V_{bw}/V_0 [Eq. (12)] above uniform flow for increasingly dense jam spacing with $L_{bw,max}/\ L_s \leq 1$, increasing jam longitudinal density and L_{bw}/L_s decreased the outflow curve skewness and outflow peak discharge [Fig. 4(a), dark blue, light blue, green, and yellow lines] and increased the outflow peak delay, relative to both inflow discharge (Fig. 4, solid black line) and outflow from an unobstructed channel [Fig. 4(a), dashed black line]. Jam arrangements with $L_{bw,max}/L_s > 1$ truncate the backwater tip, creating a trapezoidal backwater.

The jam upstream water depth was assumed to occur in the regime for which a region of falling water is present at the downstream edge of the jam, so that the upstream water depth is independent of the downstream water depth (Follett et al., 2020, 2021). Skewness of the residence time distribution of outflow discharge above base flow initially decreased [$Sk = 0.88, 0.76, 0.56, 0.22, -0.22$; Fig. 4(b)] for $L_{bw,max}/\ L_s = 0, 0.1, 0.2, 0.5, 1$, due to the increasing shallowness of the outflow discharge rising limb [Fig. 4(d); Fig. 4(a), solid yellow line]. Skewness reached an observed minimum at $L_{bw,max}/L_s = 1.25$ ($Sk = -0.36$), and continued to increase, reaching approximately $Sk = 0.958 \pm 0.009$ for $L_{bw,max}/L_s \geq 2.92$. The rate of reduction in outflow peak magnitude [Fig. 4(c)] and increase in outflow peak delay [Fig. 4(d)] decreased for spacings greater than approximately $L_{bw,max}/L_s > 2$, with both $Q_{max}/Q_{max,0}$ and $T_d/T_{d,0}$, reaching a value near $Q_{max}/Q_{max,0} = 0.726 \pm 0.009$ and $T_d/T_{d,0} = 4.49 \pm 0.04$ for jam spacings greater than $L_{bw,max}/\ L_s = 2$.

4.2. Jam accumulation factor

The impact of increasing jam accumulation factor C_A, which increases with the amount of solid wood present in the jam, was investigated for sets of 100 jams with progressively increasing C_A and decreasing h_0/h_J [$C_A \sim (h_0/h_J)^{-3}$; Eq. (8)] installed in a channel resembling the Usway Burn at Shillmoor (Table 1) with total reach length $L_R = 27610$ m including a 10 m segment downstream of the last jam at which uniform flow depth was evaluated. For example, a jam with $h_0/h_J = 0.5$ generated an upstream backwater depth twice that of the unobstructed uniform flow depth. Inflow to the channel was given by a Gaussian curve with maximum $Q = Q_{bf} = 11.83\ \mathrm{m}^3/\mathrm{s}$, minimum base flow discharge $Q = 0.2Q_{bf}$, peak inflow discharge at $\mu = 6$ hr and variance of $\sigma = 1$ hr [Fig. 5(a), solid black line]. Increasing C_A also increases L_{bw}/L_s due to the more pronounced upstream water depth, relative to uniform flow, with $L_{bw,\max}/L_s = 0.11, 0.33, 0.68, 1.0$ for conditions with $h_0/h_J = 0.75, 0.5, 0.33, 0.25$. Similar to the results of increasing L_{bw}/L_s, increasing C_A ($h_0/h_J = 0.75, 0.5, 0.33, 0.25$) increased outflow peak delay relative to time of inflow peak [$T_d/T_{d,0} = 1, 1.3, 2.2, 3.5$, Fig. 5(d)], increased reduction of outflow peak magnitude relative to outflow from an unobstructed channel [$Q_{max}/Q_{max,0} = 1, 0.98, 0.89, 0.76$, Fig. 5(c)], and decreased residence time distribution of outflow discharge above base flow [Fig. 5(b), $Sk = -0.22, 0.28, 0.78, 0.87$], yielding an increasingly gradual outflow peak rising limb.

4.3. Impact of lower gap vertical width

Jams with a lower gap allowing passage of flow under the jam are a common design for engineered logjams. Discharge approaching the jam partitions between the jam and lower gap regions, with underflow velocity and relative ratio of discharge passing through the lower gap increasing with jam accumulation factor (Follett et al., 2021). The effect of successively increasing lower gap vertical width was investigated for a channel resembling the Usway Burn at Shillmoor (Table 1), containing 100 jams spaced equally over 27600 m with $C_A = 68$, corresponding to a channel spanning jam generating $h_0/h_J = 0.25$. The total reach length was $L_R = 27610$ m including a 10 m segment downstream of the final jam. Discharge entering the reach was given by a Gaussian curve with

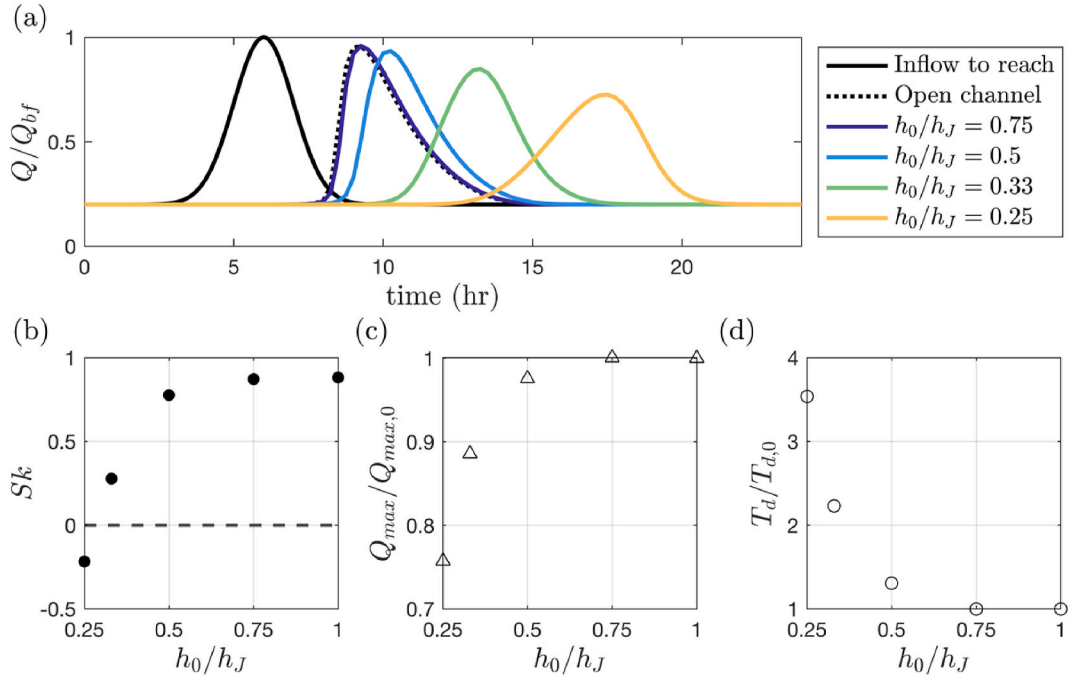

Fig. 5. Discharge entering model reach (solid black line) and outflow discharge exiting reach relative to bankfull discharge with time (h) relative to bankfull discharge. (a) Outflow hydrographs from channels with successively increasing jam accumulation factor C_A yielding $h_0/h_J = 0.75, 0.5, 0.33, 0.25$ ($C_A = 2.5, 8.5, 29, 68$), represented respectively by solid dark blue, light blue, green, and yellow curves. (b) Skewness of residence time distribution of outflow discharge above minimum base flow value $Q = 0.2Q_{bf}$ with h_0/h_J. Outflow from an open channel (no jam present) corresponds to $h_0/h_J = 1$. (c) Relative magnitude of maximum outflow discharge compared to maximum outflow discharge from an unobstructed channel $Q_{max}/Q_{max,0}$ with h_0/h_J. (d) Time delay between peak inflow and outflow discharge T_d relative to time delay for an unobstructed channel $T_{d,0}$.

maximum $Q = Q_{bf} = 11.83$ m^3/s, minimum base flow discharge $Q = 0.2Q_{bf}$, peak inflow discharge at $\mu = 6$ h and variance of $\sigma = 1$ h (Fig. 6, solid black line). Lower gap vertical width relative to channel bankfull depth $a/H_{bf} = 0.75, 0.5, 0.25, 0$ (Fig. 6, dotted black and solid dark blue, light blue, green and yellow lines, respectively) with $a/H_{bf} = 1$ (dotted black line) representing an unobstructed channel and $a/H_{bf} = 0$ (solid yellow line) representing a channel-spanning jam. The relative discharge at which uniform flow depth in the channel reached the jam lower edge was equal to $Q_a/Q_{bf} = (a/H_{bf})^{3/2} = 0.65, 0.35, 0.13, 0$, respectively, shown by thin black solid, dashed, and dot dash horizontal lines for cases with $a/H_{bf} = 0.75, 0.5, 0.25$ in Fig. 6(a). The stage-discharge relationships for jams with lower gap width $a/H_{bf} = 0.75, 0.5, 0.25$ (solid dark blue, blue, and green lines) as compared to unobstructed flow (dashed black lines) are respectively shown in Fig. 6 (b)–(d).

Decreasing lower gap vertical width also increased the maximum backwater length for the inflow discharge tested, with $L_{bw,max}/L_s = 0.10, 0.26, 0.55, 1.00$ for $a/H_{bf} = 0.75, 0.5, 0.25, 0$. Outflow peak delay, reduction in peak magnitude, and skewness increased with decreasing lower gap vertical width, with $T_d/T_{d0} = 1.08, 1.38, 2.15, 3.54$, $Q_{max}/Q_{max,0} = 1.00, 0.97, 0.88, 0.76$ and $Sk = 0.88, 0.57, -0.49, -0.22$, respectively for $a/H_{bf} = 0.75, 0.5, 0.25, 0$. The smallest lower gap width tested, $a/H_{bf} = 0.25$, which was submerged at the minimum inflow level, had reduced outflow peak delay and peak magnitude reduction compared to the series of channel-spanning jams [Fig. 6(a)], and a more pronounced decreased skewness. For cases where the water depth reached the jam lower edge during passage of the inflow wave [Fig. 6(a), light and dark blue lines], outflow discharge tracked the curve for the unobstructed case (thick dotted black line in Fig. 6) until flow depth reached the jam lower edge [Fig. 6(a), horizontal dashed and solid lines corresponding to solid light blue and solid dark blue cases, respectively]. For discharge values above this point, delay of the outflow curve increased relative to the unobstructed case, and a reduction in peak magnitude was observed.

4.4. Local overflow to floodplain

Jams that generate an upstream depth higher than the channel bankfull depth generate local inundation of the surrounding floodplain [Fig. 1(b)]. The flow pathways are highly complex and dependent on local topography. As a first step in estimating the effect of jam-generated upstream depths above bankfull level and local inundation, a compound channel was used to represent the local floodplain [Fig. 7(a) and (b)]. Discharge above the upstream bankfull depth was assumed to pass over the jam similar to flow over a weir (Hankin et al., 2020). Two methods were used to investigate the effect of jams with a finite vertical extent. Jams with top edge elevation $H_J = 1.5H_{bf}$ (Case A) were assumed to occupy a local floodplain width of $B_{eff} = 3B_{bf}$ at elevations above the channel bankfull depth, with discharge that overtopped the jam top edge represented by a weir [Fig. 7(a)]. Jams with top edge elevation $H_J = H_{bf}$ (Case B) were assumed to inundate a local floodplain of width B_{bf} on either side of the channel ($B_{eff} = 3B_{bf}$) represented by uniform flow with floodplain resistance $n_0 = 0.1$, with discharge passing over the jam top edge represented by a weir [Fig. 7(b)]. Tested channel properties corresponded to the Usway Burn at Shillmoor (Table 1), containing 200 jams spaced equally over 10720 m with $C_A = 8.5$, corresponding to a channel spanning jam generating $h_0/h_J = 0.5$. In both cases, jams had a lower gap of vertical width $a = 0.5H_{bf}$ [Fig. 7(c)]. The total reach length was $L_R = 10730$ m including a 10 m unobstructed segment downstream of the final jam. Discharge entering the reach was given by Gaussian curves with minimum base flow discharge $Q = 0.2Q_{bf}$, peak inflow discharge at $\mu = 6$ hr and variance of $\sigma = 1$ hr, with varying maximum discharge $Q_{max}/Q_{bf} = 0.5, 1, 1.5, 2$ with $Q_{bf} = 11.83$ m^3/s [Fig. 7(d) and (e), dashed dark blue, light blue, green, and yellow lines].

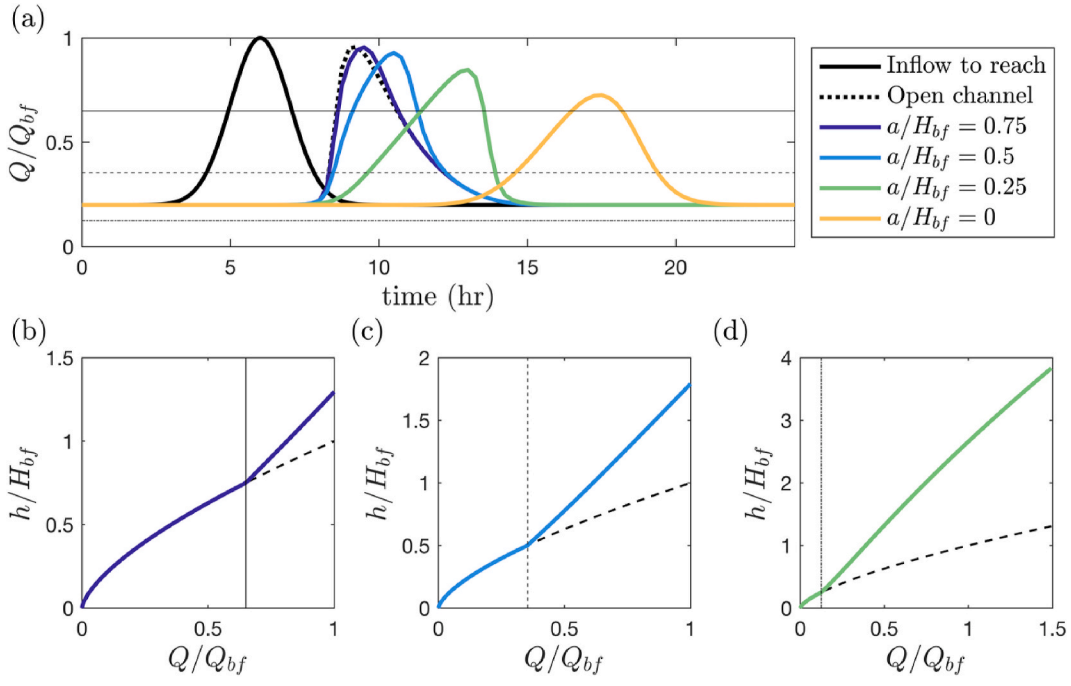

Fig. 6. (a) Discharge entering model reach (solid black line) and outflow discharge exiting reach relative to bankfull discharge with time (h). Outflow from an unobstructed channel (dotted black line) and channels containing 100 jams with successively decreasing vertical width of lower gap relative to channel bankfull depth $a/H_{bf} = 0.75, 0.5, 0.25, 0$ represented respectively by solid dark blue, light blue, green, and yellow curves, with $a/H_{bf} = 0$ (solid yellow line) representing a channel-spanning jam. Solid gray, dashed gray, and dotted gray lines correspond to discharge at which water depth reaches jam lower edge for $a/H_{bf} = 0.75, 0.5, 0.25$, respectively. (b,c,d) Stage-discharge curves for jam-generated upstream water depth relative to bankfull channel depth (solid dark blue, light blue, green lines for $a/H_{bf} = 0.75, 0.5, 0.25$, respectively) and unobstructed uniform flow relative to bankfull depth (black dashed lines) with discharge relative to bankfull discharge. Thin vertical solid, dashed and dotted lines represent discharge at which water depth reaches jam lower edge for $a/H_{bf} = 0.75, 0.5, 0.25$, respectively.

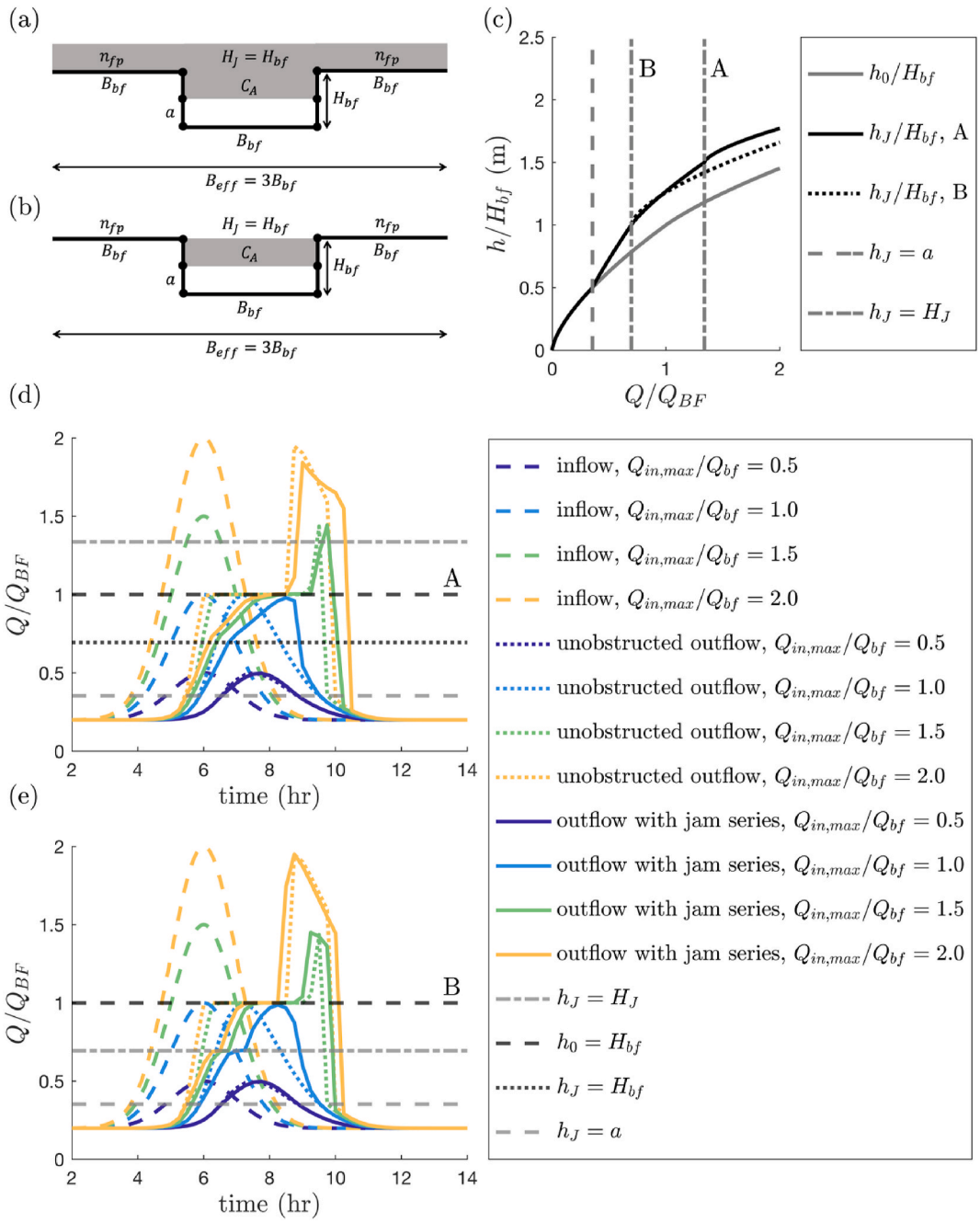

Fig. 7. (a) Jam case A with elevation of jam top edge $H_J = 1.5H_{bf}$, with jam extending the total width of the local floodplain ($B_{fp} = 3B$) above the channel bankfull depth. (b) Jam case B with elevation of jam top edge $H_J = H_{bf}$ equal to the channel bankfull depth, with local floodplain width assumed to be equal to the channel bankfull width on either side of the channel and floodplain resistance equal to $n_0 = 0.1$. (c) Water depth relative to bankfull depth with discharge relative to bankfull depth. Jam-generated upstream depth for cases A and B respectively represented by black solid and dotted lines. Uniform flow depth represented by solid gray line. Relative discharge at which jam-generated upstream depth reaches jam bottom and top edges respectively represented by gray dashed and dash-dot lines. (d,e) Discharge entering model reach (dashed lines) and outflow discharge exiting reach relative to bankfull discharge with time (hr) for a reach with 200 jams (solid lines) and an unobstructed reach (dotted lines). Line color represents successively increasing $Q_{max}/Q_{bf} = 0.5, 1, 1.5, 2$ respectively represented by solid dark blue, light blue, green, and yellow lines.

In both cases, outflow discharge from a channel containing jams was delayed relative to outflow discharge from an unobstructed channel for sub-bankfull discharge levels [Fig. 7(d) and (e), light blue solid and dashed lines], due to the relative increase in jam-generated upstream depth above the point of inundation of the jam lower edge [Fig. 7(d) and (e), horizontal dashed gray line] and inundation of the simplified local floodplain for jam-generated upstream depths above bankfull depth [Fig. 7(d), dotted black to dashed black horizontal lines and Fig. 7(e), dash-dot gray to dashed black horizontal lines]. The maximum observed relative peak delay between outflow from a channel with and without jams occurred for a tested maximum discharge of $Q/Q_{bf} = 1$, which generated a relative time delay in peak outflow of $T_d = 1.25$ hr for Case A [Fig. 7(d), $Q_{max} = 0.98Q_{bf}$] and $T_d = 1$ hr for Case B [Fig. 7(e), $Q_{max} = 0.99Q_{bf}$]. In both cases, inflow discharge below the point of inundation of the jam lower edge had no effect on outflow discharge relative to an unobstructed channel [Fig. 7(d),(e), dashed gray and dark blue solid and dotted lines). Above bankfull discharge [Fig. 7(d) and (e), horizontal black dashed line], the effect of jams was reduced as unobstructed flow

also experienced a delay relative to in-channel flow due to the increased effective channel width $B_{eff} = 3B_{bf}$ and floodplain roughness. The magnitude of outflow discharge for the highest inflow discharge curve tested was slightly reduced relative to outflow from an unobstructed channel for Case A (95% of unobstructed outflow maximum), but negligible for Case B as the jam became overtopped at only $Q/\ Q_{bf} = 0.69$ [Fig. 7(e), horizontal gray dash-dot line], so that the effect of the jam was reduced for higher discharge levels. The simplified compound channel representation is not sufficient to reproduce the complex flow paths observed in natural overflow conditions [Fig. 1(b)], and additional research is needed to understand the effect of jam installations at above-bankfull discharge levels and interaction between jams and local floodplain flows.

4.5. Channels of varying slope

Placement of the same jam in channels of increasing slope would be expected to result in relatively higher backwater rise and backwater volume above uniform flow [Eq. (12), Fig. 4], but reduced backwater length for a given (h_J, h_0) due to increasing S. For channels resembling the Chittern at Codford, Usway Burn at Shillmoor, and Burbage Brook at Burbage (Table 1) with $L_R = 19768$ m with jams spaced over 19758 m, the effect of identical series of $N = 200$ jams with constant $C_A = 29.5$, lower gap width $a = 0.5H_{bf}$ and spacing $L_s = 98.79$ m [Fig. 8(a)–(c), solid light blue lines], and jam series with constant $h_0/h_J = 0.33$ ($C_A = 53.6,\ 29.5,\ 12.1$, respectively), lower gap width $a = 0.5H_{bf}$ and maximum $L_{bw}/L_s = 1$ ($L_s = 121.96, 40.57, 20.75$ m; $N = 162, 487, 952$ jams, respectively) [Fig. 8(a)–(c), solid dark blue lines] were explored relative to outflow discharge from an unobstructed channel [Fig. 8(a)–(c), solid gray lines]. In all cases, inflow to the channel had maximum discharge $Q/Q_{bf} = 1$ and minimum $Q/Q_{bf} = 0.2$, for a Gaussian curve with peak inflow discharge at $\mu = 6$ hr and variance of $\sigma = 1$ hr. Jams had top elevation $H_J = 1.5H_{bf}$ with an estimated local floodplain width of B_{bf} ($B_{eff} = 3B_{bf}$) on either side of the channel and floodplain resistance $n = 0.1$ [case A, Fig. 7(a)].

Outflow from jam series with constant C_A, N and L_s showed a higher relative effect for the lowest slope channel [Fig. 8(a), light blue solid line compared to light blue solid lines in Fig. 8(b),(c)]. An increase in time delay of outflow discharge peak and reduction in outflow peak magnitude was observed, relative to outflow from an unobstructed channel [Fig. 8(a), solid gray line]. For channels with increasing slope resembling the Chittern at Codford, Usway Burn at Shillmoor, and Burbage Brook at Burbage, respectively, time delay relative to outflow from an unobstructed channel was $T_d = 3.25, 2.5, 0.5$ hr and relative reduction in outflow peak magnitude was $Q_{max}/Q_{max,0} = 0.80, 0.93, 0.99$. In all cases, little delay in outflow discharge relative to an unobstructed channel was observed for discharge levels below the point of inundation of the jam lower edge (Fig. 8, horizontal dashed gray line). Relative delay of outflow discharge increased for discharge levels corresponding to jam-generated upstream depths above bankfull level, which caused inundation of the simplified local floodplain [Fig. 8(a)–(c), dashed light and dark blue lines] For the highest slope channel tested [Fig. 8(c)], the jam overtopped at $Q/Q_{bf} = 0.76$, which reduced relative peak delay and reduction in peak magnitude [Fig. 8(c),(f), dash dot light blue line].

Outflow from the jam series with constant $h_0/h_J = 0.33$ and $L_{bw}/L_s = 1$ for all channels [Fig. 8(a)–(c), solid dark blue lines] showed a more consistent effect across all channels for discharge levels, with $T_d = 3.5$, 3.5, 4 hr and $Q_{max}/Q_{max,0} = 0.77, 0.76, 0.81$ respectively for test

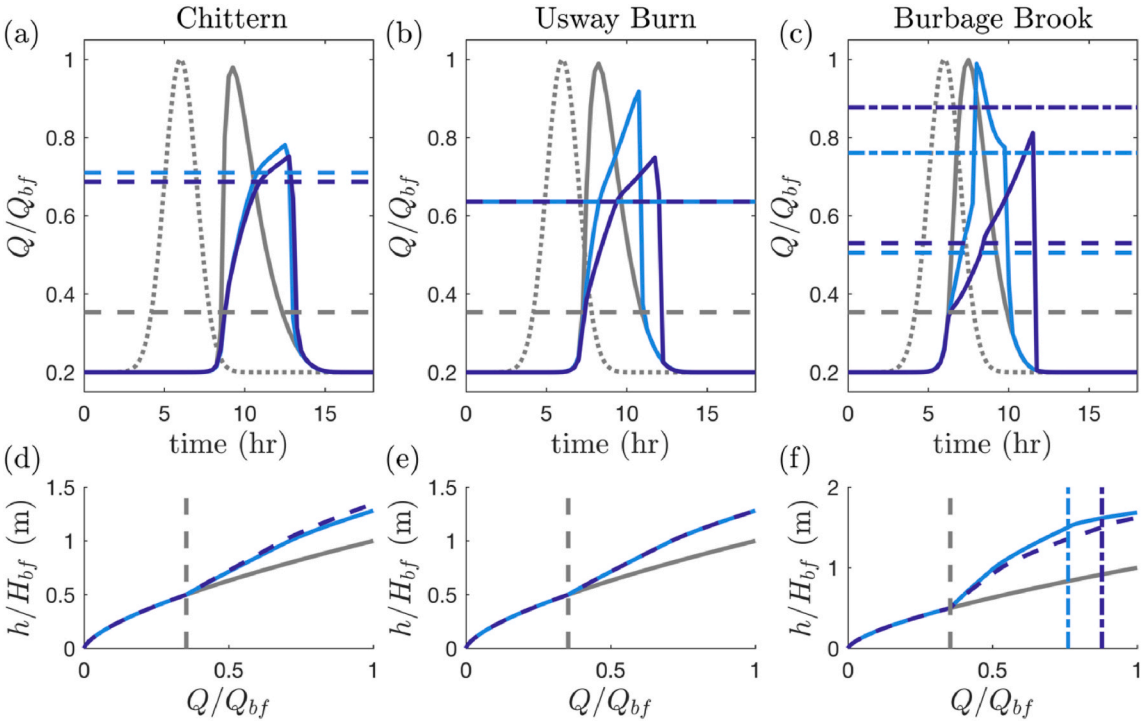

Fig. 8. (a)-(c) Discharge entering model reach (dashed gray line) and outflow discharge exiting reach relative to bankfull discharge relative to bankfull flow $Q/\ Q_{bf}$ with time (hr) for channels resembling the Chittern, Usway Burn, and Burbage Brook, respectively (Table 1). Relative discharge exiting an unobstructed channel represented by solid gray line. Light blue solid line represents relative discharge exiting channel of $L_R = 19768$ m with 200 jams with $C_A = 29.5$ spaced $L_s = 98.79$ m apart over 19758 m. Dark blue solid line represents relative discharge exiting channel of $L_R = 19768$ m with $N = 162, 487, 952$ jams spaced over 19758 m, with relative ratio $h_0/h_J = 0.33$ for all channels [$C_A = 53.6, 29.5, 12.1$, respectively for cases (a)-(c)]. Horizontal dashed light and dark blue lines indicate relative discharge at which jam-generated upstream depth reached channel bankfull depth. (d)-(f) Unobstructed flow depth (gray solid line), water depth upstream of jam with $C_A = 29.5$ (solid light blue line), and upstream water depth generated by jam with $h_0/h_J = 0.33$ ($C_A = 12.1, 29.5, 53.6$, respectively for (d)-(f); dashed dark blue line) relative to channel bankfull depth, with channel relative discharge. In all cases, dashed gray lines indicate the value of Q/Q_{bf} at which the jam-generated upstream depth reached the jam lower edge. For figures (c),(f), dash-dot light and dark blue lines indicate relative discharge value at which jam became overtopped.

channels with increasing slope. The increase in peak delay and reduction in outflow discharge magnitude occurred for channels with both an increase in C_A and reduction in number of jams [Fig. 8(a), $N = 162$ and $C_A = 53.6$ for solid dark blue line, $N = 200$, $C_A = 29.5$ for solid light blue line, $L_{bw,max}/L_s = 1$ in both cases], increase in number of jams and $L_{bw,max}/L_s$ with constant C_A [Fig. 8(b), $L_{bw,max}/L_s = 0.41$ for solid light blue line, $L_{bw}/L_s = 1$ for solid dark blue line], and reduction in C_A with increase in number of jams and L_{bw}/L_s [Fig. 8(c), $C_A = 29.5$, $L_{bw}/L_s = 0.23$ for solid light blue line, $C_A = 12.06$, $L_{bw}/L_s = 1$ for solid dark blue line]. Although the jams would have become overtopped for the highest inflow discharge levels at Burbage Brook [$Q_{max}/Q_{max,0} = 0.88$, dash dot dark blue line in Fig. 8(c),(f)], the maximum outflow discharge fell below this level and the outflow discharge profile more closely resembled cases where jam overtopping was not observed, with an increase in relative delay both above the point of inundation of the jam lower edge [Fig. 8, horizontal dashed gray line] and discharge level corresponding to point at which jam-generated upstream depth reached the channel bankfull depth [Fig. 8(c), horizontal dashed dark blue line].

4.6. Best-fit effective resistance coefficient

Use of an elevated resistance coefficient to represent a series of jams is of interest for larger scale modelling and scenarios for which individual representation of jams is prohibitively time-consuming or raises issues with model stability. For the same discharge, an elevated channel resistance increases water depth uniformly across the full channel segment length, in contrast to the triangle-like backwater shape generated by a jam (Fig. 2). For this reason, a best-fit elevated resistance model fit to the outflow hydrograph from a series of jams can approximate the time delay and reduction in peak magnitude found from outflow from a series of jams, but does not reproduce the reduction in outflow peak skewness, where this is observed [Fig. 4(a)]. In addition, channel segment water volume and overflow to the local floodplain would differ between the individual jam and best-fit resistance models. The degree of elevation in channel resistance increased with decreased inter-jam spacing. Elevated resistance was bounded on the lower end by an unobstructed channel (C_{f0}) and on the upper end by a resistance generating $H = h_J$ across the full channel length ($C_{fe,max}$). For a channel-spanning jam with no lower gap, the maximum resistance was equal to the cube of the relative ratio of the jam-generated upstream depth and unobstructed uniform flow depth $C_{fe,max}/C_{f0} = (h_0/h_J)^{-3}$. The best-fit effective elevated resistance that minimized difference in outflow from a channel with elevated bed resistance and outflow from a channel with a series of channel spanning jams in an infinitely deep channel was found for the Usway Burn at Shillmoor for $N = 10$, 25, 50, 100, 125, 150, 200, 292 jams (Section 4.1). The ratio between the difference in effective resistance and unobstructed resistance and difference between maximum and unobstructed resistance increased with increasing $L_{bw,max}/L_s$ [Fig. 9(a)]. Due to the increasing shallowness of the outflow hydrograph rising limb generated by the triangular backwater, the difference between the outflow modelled by a best-fit effective resistance coefficient and outflow from a series of jams increased with decreasing inter-jam spacing, up to $L_{bw,max}/L_s = 1$ [Fig. 9(b)]. After this point, truncation of the backwater tip created a trapezoidal backwater, decreasing the difference between the best-fit resistance and jam series curves. The upper bound for effective resistance assuming that $H = h_J$ everywhere in the channel (corresponding to $y = 1$ in Fig. 9(a)) at $h_J = H_{bf}$ [Fig. 9(c), black open circles] and channel depth-average upper bound for effective resistance at $h_J = H_{bf}$ [Fig. 9(c), blue open circles] decreased with increasing relative gap width.

5. Discussion

5.1. Comparison of modelled jam trends with field observations

Jam presence has been observed to increase reach mean depth and decrease reach mean velocity (Linstead and Gurnell 1999), due to the formation of a jam-generated upstream backwater. The aggregate effect of a series of jams has been observed to attenuate upstream flood peaks and increase flow travel time, contributing to downstream flood attenuation (Gregory et al., 1985; Linstead and Gurnell 1999; Dadson et al., 2017). Consistent with this expectation, a series of jams placed in a modelled 1D channel increased the peak delay and peak outflow discharge magnitude of an inflow discharge wave, relative to an unobstructed channel with the same channel length, slope, width, and bed resistance (Fig. 4). The increase in outflow peak delay and reduction in peak magnitude was consistent with previous modelling results for increasing numbers of jams in a channel (Metcalfe et al., 2017). Consistent with the modelled increase in effective optimum bed resistance due to a series of jams relative to unobstructed bed resistance (Fig. 9), Linstead and Gurnell (1999) measured elevated Manning's n with increasing discharge (Linstead and Gurnell 1999, Fig. 2.5 in that paper) for two reaches in the Forest of Dean, Gloucestershire that contained active jams observed to span the full channel extent and generate an observable change in water surface profile. All recorded flows were in-channel. Following jam removal, measured Manning's n decreased for all discharge values. The increased, effective measured Manning's n ranged from 1.7 to 2.2 times above the unobstructed Manning's n value. This increase in n_e/n_0 would correspond to a theoretical maximum channel resistance of $C_{f,e}/C_{f,0} = (n_e/n_0)^2 = 4$, consistent with a series of

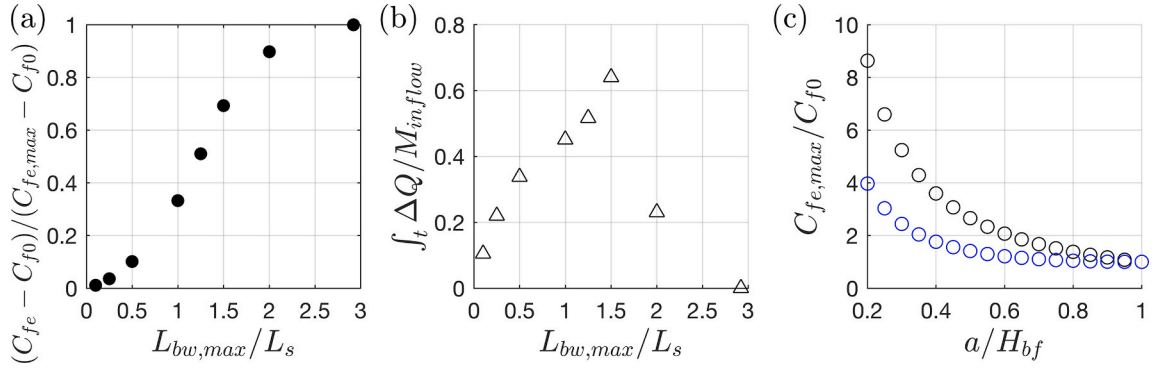

Fig. 9. (a) Ratio between the difference in optimum effective resistance and unobstructed resistance and difference between maximum and unobstructed resistance increased with increasing $L_{bw,max}/L_s$ for $N = 10$, 25, 50, 100, 125, 150, 200, 292 channel-spanning jams. (b) Integrated difference in outflow discharge relative to mass of inflow discharge above base flow for a series of $N = 10$, 25, 50, 100, 125, 150, 200, 292 jams and jams modelled with a best-fit resistance coefficient that minimized difference in outflow discharge curves. (c) Upper bound for effective resistance relative to unobstructed resistance with increasing relative gap height a/H_{bf}, assuming $H = h_J$ everywhere in the channel. Maximum effective resistance (black open circles) and channel depth-average effective resistance (blue open circles) shown for $h_J = H_{bf}$. In all cases channel properties resembled the Usway Burn at Shillmoor (Table 1).

closely spaced jams generating a relative upstream depth 1.6 times the unobstructed uniform flow depth, with $h_0/h_J = 0.63$.

Guidance for design of leaky barriers (Wren et al., 2022, YDRT 2021) suggests a spacing of approximately 7 channel widths for a jam with a lower gap vertical width of approximately 0.3 m extending to approximately 1.5 times the channel bankfull depth (Wren et al., 2022, YDRT 2021). The recommended channel spacing was compared to model estimations for a jam accumulation that would have generated $h_0/\ h_J = 0.5$ if arranged with no lower gap. For the three channels considered with varying $S = 0.001935, 0.008479, 0.021467$, (Table 1, Hey and Thorne 1986), bankfull depth was relatively consistent across all sites ($H_{bf} = 0.68, 0.78, 0.72$ m, Table 1). A lower gap vertical width of 0.3 m would result in relative gap width $a/H_{bf} = 0.44, 0.38, 0.42$, similar to the $a/H_{bf} = 0.5$ case shown with a solid light blue line in Fig. 6. The backwater length when jam-generated upstream depth was equal to channel bankfull depth was reduced from the case with no lower gap, with backwater length relative to channel bankfull width equal to $L_{bw}/B_{bf} = 10.9, 2.7, 2.1$ respectively for channel sites with increasing slope. For the two higher slope cases, the modelled backwater length was smaller than the recommended spacing of 7 channel widths. The rate of increase in the time delay of the outflow discharge peak and reduction in outflow discharge peak magnitude relative to outflow from an unobstructed channel reduced for spacings closer than approximately $L_{bw,max}/L_s = 1-1.5$ (Fig. 4), suggesting that placement of additional jams to generate a spacing closer to the maximum expected backwater length could result in additional time delay of the outflow discharge peak and relative reduction in peak magnitude. The simplified 1D scenarios considered in this paper assessed the effect of a series of jams with varying jam and channel physical properties. While the model framework allows for provision of lateral inflow along the modelled reach, lateral inflows were not considered in the test cases considered. To accurately assess the implications of jam installation in larger catchments, future work should consider the addition of lateral inflow and catchment-scale hydrological effects, such as that generated by a catchment-scale hydrological model (Metcalfe et al., 2017, Lewis et al., 2018). In addition, the sensitivity of outflow characteristics to temporal change of jams due to seasonal build-up and loss of wood and leaf material and floodplain morphology should be considered in future modelling and empirical studies.

Black et al. (2020) observed an increase in outflow peak lag time compared to prior baseline measurements of the same channel before installation of a series of leaky barriers in the Middle Burn (35 leaky barriers) and Craigburn (44 leaky barriers), alongside riparian and wetland tree planting and, in the case of Craigburn, construction of three offline holding ponds. Lag time was observed to increase with flood magnitude up to approximately QMED, or bankfull flow. The increase in peak lag time within this range was attributed to the design of structures that allowed increased passage of water at low flows, similar to jams with a lower gap considered in this paper, for which a relative increase in delay of outflow discharge relative to an unobstructed channel was observed for discharge values above the inundation point of the jam lower edge, compared to lower flow values (Fig. 6). For the largest events measured with discharge level above QMED, median lag continued to rise at a reduced rate at Middle Burn, but decreased sharply to near pre-installation values at Craigburn. In both cases the relative peak lag for events above QMED was reduced relative to sub-QMED events (Black et al., 2020, Fig. 3 in that paper). The change at near-bankfull flow is consistent with model output with a simplified channel-floodplain configuration (Fig. 8) showing reduced peak lag for increasing peak inflow discharge, as water level began to inundate the model floodplain and in some cases overtop the modelled jams. Prior modelling studies of vegetated channels have shown a similar reduction in sensitivity to vegetation-generated roughness for larger floods, compared to smaller flood inputs (Anderson et al., 2006). Despite an increased number of interventions at Craigburn, the observed increase in peak lag time was observed to be less than at Middle Burn, which was attributed to likely variation in barrier physical properties and placement, channel gradient, and differences in geology, surface cover, and soil composition (Black et al., 2020).

5.2. Recommendations for jam design in varying channels

Identical jams placed in channels of increasing slope would be expected to generate a higher relative backwater rise and backwater volume above base flow V_{bw}/V_s (Fig. 3), but lower backwater length $L_{bw} = (h_J - h_0)/S$. For the same set of jams placed with equal spacing in low, medium, and high slope channels of the same modelled length (Table 1, Fig. 8), a more pronounced outflow delay associated with jam presence was observed for the lowest slope site, due to higher L_{bw}/L_s compared to the higher slope cases. Existing guidance recommending placement at approximately 7–10 channel widths (Linstead and Gurnell 1999; YDRT 2021) in part incorporates the effect of increasing slope as bankfull width is expected to decrease with increasing slope (Parker et al., 2007). However, the observed empirical scaling of $B_{bf} \sim S^{-0.4}$ was weaker than the inverse linear dependence of backwater length on slope (Parker et al., 2007, Section 2.4). Similarly, across the 3 example sites, the decrease in bankfull depth was less strong than the decrease in backwater length, so that a jam with no lower gap generating $h_0/h_J = 0.5$ would generate a backwater length relative to bankfull depth $L_{bw}/B_{bf} = 27, 5,$ and 3 channel widths, respectively for sites with $S = 0.001935, 0.008479, 0.021467$ (Table 1) when the jam-generated upstream depth was equal to the channel bankfull depth.

Jams spaced more closely than $L_{bw,max}/L_s = 1$ had reduced increase in time delay of outflow peak and reduction in peak magnitude with L_{bw}/L_s, suggesting that closer jam spacings than $L_{bw,max}/L_s = 1$ may generate reduced attenuation per jam, and provide less value per money. However, magnitude of time delay of outflow peak and magnitude of reduction in outflow peak magnitude continued to increase for more closely spaced jams, until the point at which the jam backwater would have reached the adjacent upstream jam even at the minimum inflow discharge.

In cases with a simplified model floodplain that allowed for jam overtopping, the effect of jams was increased when jam-generated upstream depth exceeded bankfull depth for unobstructed sub-bankfull discharge values, but reduced for discharge values that overtopped the jam. Reducing jam accumulation factor to delay overtopping and implementing jam installations in conjunction with riparian forest planting or other measures to increase local floodplain resistance (Black et al., 2020), may help to attenuate higher flood levels. Similarly, jams with a lower gap had no effect at discharge levels for which the water depth would not have reached the jam lower edge, and reduced outflow peak time delay and reduction in peak magnitude compared to jams with no lower gap. However, the presence of the lower gap increased the discharge value at which the jam became overtopped, allowing a wider upper range of jam-generated effect on outflow discharge.

5.3. Leaky Barrier Advisor

As interest in nature-based solutions for natural flood management and sustainable farming has increased, interest has grown in sparse input data methods suitable for participatory modelling including incorporation of lay knowledge and site observations collected by farmers, government regulators, and citizen scientists (Voinov and Bousquet 2010; Basco-Carrera et al., 2017; Voinov et al., 2016; Hedelin et al., 2021). The simplified 1D network model described in this paper (Section 3.2) can be used to estimate the effect of jam installations on an inflow hydrograph using channel slope, bankfull width, and site observations of jam relative gap width a/H_{bf}, relative h_0/h_J, or related observations such as the amount of times per year that the channel bank became inundated upstream of the jam, relative to downstream or unobstructed flow. For sites with unknown bankfull depth, D_{s50} and bed

friction coefficient, channel slope and bankfull width can be used to estimate H_{bf}, D_{s50}, and C_{f0} [Eqs. (3)–(5)]. While the model capabilities lack a catchment scale hydrological model and are limited relative to standard hydraulic modelling software packages, model set-up time and runtime are reduced, and a range of jam and channel properties can be trialled with relatively sparse data input. After computing outflow discharge from a given inflow and specified channel and barrier properties, inflow and outflow hydrographs are plotted in addition to jam-generated upstream water depth as compared to unobstructed uniform flow depth over the range of the inflow hydrograph.

5.4. Example implementation in HEC-RAS 2D

To demonstrate implementation of jams as hydraulic structures and the theoretical maximum effect of jam implementation using the maximum equivalent channel resistance (Section 4.6, $h = h_J$ everywhere in the channel), modelled and measured outflow were compared for a channel containing eight engineered logjams (Penny Gill, West Cumbria, UK) within a small catchment area of approximately 0.33 km^2. Measured outflow discharge recorded for a rain event occurring over 48.25 h between 14:30, March 9, 2021–14:45, March 11, 2021, downstream of eight engineered jams and a series of scattered wood pieces. Based on the Revitalised Flood Hydrograph (Kjeldsen et al., 2005) the event is estimated as having an Annual Exceedance Probability of approximately 20%, although with such an incised channel in places this does not equate to significant out of bank flow in the study reach. Reach sections were measured at $x = 0, 40, 100, 205, 215, 259, 276, 320, 344,$ 419 m from the reach upstream edge with elevation $z = 60.23, 58.23,$ $52.35, 46.96, 46.04, 43.2, 42.18, 40.6, 38.17, 33.67$ m and channel width $B = 4, 4, 7, 5.8, 5.2, 4.9, 4.2, 6, 3.8, 3.8$ m. Jams were located on sections 2-7, 9, and 11. The jam upper edges were $H_J = 0.86, 0.86, 0.97, 1, 1.12,$ $1.09, 0.83, 1.04$ m above the bed. The unobstructed channel resistance was estimated to equal $n_0 = 0.23$ s m$^{-1/3}$, based on observations of rough channels with scattered wood pieces (Yochum et al., 2014).

In separate model runs, jams were represented both as individual hydraulic structures and using an effective Manning's resistance coefficient using HEC-RAS 2D. Individual jams were represented as embankments spanning the channel with a custom outlet rating curve, assuming the jams acted as channel-spanning jams with no lower gap [Eq. (7)]. A jam accumulation factor of $C_A = 50$ was estimated from an available photograph [Fig. 1(a)], assuming that the structure was approximately 1 m high with five cylindrical logs of equal diameter. The estimated C_A (Follett et al., 2020) ranged from $C_A = 64 - 43$ depending on chosen inter-log gap width of 1–2 cm, respectively. $C_A = 50$ was chosen based on this range, yielding a relative ratio of unobstructed flow depth to jam-generated upstream depth $h_0/h_J = 0.42$. In addition to model runs including individual jams, an effective Manning's resistance coefficient was chosen ($n_e = 0.24$) to minimize the difference between outflow modelled with an elevated resistance coefficient and eight individual jams, and the limiting maximum resistance $n_{e,max} = 0.68$ was computed assuming average channel properties $S = 0.054, n_0 = 0.23$ s m$^{-1/3}$, $C_A = 50$ with C_{f0} related to n_0 assuming a channel bankfull depth of 1 m and average $B = 5.1$ m.

The HEC-RAS 2D model mesh had an average spacing of 4 m with sub-grid topography of 1 m. Model results are shown for 10:30 March 10, 2021–14:45 March 11, 2021 following an initial period in which depressions in the 2D domain adjusted to inflow. Conservation of mass and momentum were solved over the model domain using the diffusion wave approximation of the shallow water equations. Solution using the full momentum equations was tested, but did not significantly alter model results.

The effect of jams was limited for the site and event considered due to the low maximum discharge (maximum $Q = 0.22$ m^3 s^{-1} corresponding to $h_0 = 0.125$ m in an unobstructed channel), high unobstructed channel resistance, and small number of jams. Modelled outflow curves were higher than measured outflow for the rising limb of the initial, smaller peak (Fig. 10, $t = 14:30 - 16:30$, 10 March 2021) and lower than measured outflow for the falling limb of the main peak (Fig. 5, $t = 22:00$, 10 March 2021 $- 04:30$, 11 March 2021). The outflow discharge modelled using individual jam hydraulic structures (green dash dot line in Fig. 10) was lower than the measured outflow discharge and curves modelled using a bed resistance (Fig. 5, $t = 10:30 - 14:30$, 17:30–21:00, 10 March 2021, 01:00–11:30, 11 March 2021), which may be due to model uncertainty related to low water depth ($h_0 = 0.02$ m for uniform flow, $Q = 0.005$ m^3 s^{-1}) and the presence of vertical lower gaps below some jams. The discrepancy at low water depths reduced the model Nash-Sutcliffe Efficiency $\left[NSE = 1 - \frac{\sum_t (Q_m - Q_{obs})}{\sum_t (Q_{obs} - \overline{Q_{obs}})}\right]$ to $NSE = 0.73$ for the model run using eight individually represented jams from $NSE = 0.78$ for the model run using an effective resistance coefficient. The analytical maximum resistance $n_{e,max} = 0.68$, which was computed assuming $h = h_J$ everywhere in the channel, reduced the outflow peak magnitude ($Q_{max}/Q_{max,obs} = 0.763$) and increased time delay $T_d = 0.25$ hr to first peak relative to measured outflow, showing the maximum possible effect of many jams installed in the channel.

6. Conclusion

Logjam representation in hydraulic modelling schemes is used in industry to predict the effects of natural flood management project designs. Further modelling and empirical studies are needed to assess the performance of engineered logjam installations and interpret field monitoring results. While recent results have demonstrated that a jam can be modelled as a porous obstruction generating momentum loss proportional to the number, size, and packing density of the logs and the jam length, providing a physically based stage-discharge relationship (Follett et al., 2020, 2021), representation of many jams as hydraulic structures increases model set-up time and runtime, and approximation of jam effects with an increased channel resistance provides a practical alternative (Addy and Wilkinson 2019). Field observations suggest that jams increase time delay of the outflow peak and reduce outflow peak magnitude relative to baseline measurements, but that a range of effects are present due to dependence on jam and site characteristics, including channel slope and bed resistance (Black et al., 2020).

To systematically investigate the effect of a series of logjams with varying channel and jam physical properties, we represented a rectangular channel containing jams with a 1D network (Hankin et al., 2020). The relative time delay of the outflow peak and relative reduction in peak magnitude increased with number of jams in the channel, which increased the relative ratio of backwater length to segment length. Skewness of the outflow discharge curve initially decreased with increasing relative backwater length to segment length, generating an increasingly gradual outflow discharge rising limb. As jams became more closely spaced than one backwater length, a trapezoidal backwater was generated, and the outflow discharge from a series of jams more closely resembled that from a channel with elevated bed resistance. The maximum equivalent channel resistance generated by a series of jams would occur when $h = h_J$ everywhere in the channel, generating a relative effective resistance coefficient $C_{fe}/C_{f0} = (h_0/h_J)^{-3}$ for a series of channel-spanning jams with no lower gap. The analytical maximum equivalent resistance could be used to quickly estimate the maximum possible effect of a series of jams at a given site, although both the best-fit equivalent resistance and the deviation of a resistance model from a jam series decline with increased jam spacing.

The model described in this paper provides a sparse data input option suitable for use with site observations of the relative water depths generated by a jam and estimation of channel slope and bankfull depth, which could be used to explore the implications of varying jam spacing and design or estimate the effect of existing jam installations. To demonstrate implementation of best-fit and maximum elevated channel

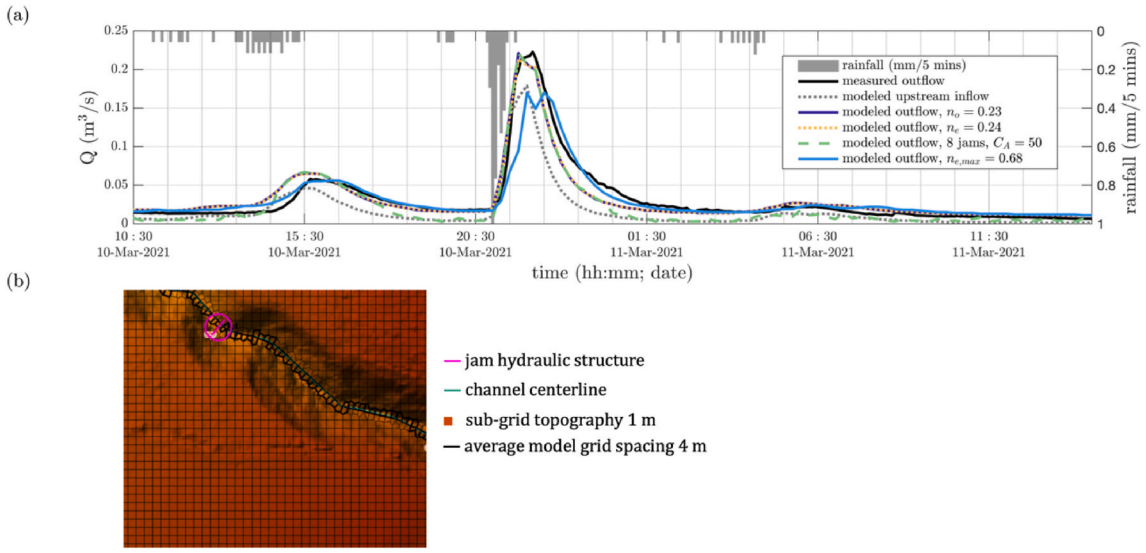

Fig. 10. (a) Model setup showing upper part of Penny Gill, West Cumbria, UK, highlighting how each of 8 larger jams were represented as an embankment spanning the channel with a custom outlet rating curve based on Eq. (7) and $C_A = 50$. Model mesh had average spacing 4 m with sub-grid topography of 1 m. (b) Field observations and model results for Penny Gill, West Cumbria, UK (10:30 March 10, 2021–14:45 March 11, 2021). Date and time of observations and model results shown at same scale for both top and bottom x-axes. Modelled net rainfall (mm) used as input to HEC-RAS 2D model shown with gray dotted line on right-hand y-axis and top x-axis. Observed discharge recorded downstream of eight jams shown with black solid line on left y-axis and bottom x-axis. Modelled inflow to upstream section shown with dashed gray line. Modelled HEC-RAS 2D outflow without jams, including the effect of scattered logs in the channel ($n_0 = 0.23$ s m$^{-1/3}$) shown with solid dark blue line. Modelled HEC-RAS 2D outflow representing the effective increase in n due to jam presence ($n_e = 0.24$ s m$^{-1/3}$) shown with dotted yellow line. Modelled outflow with channel resistance set at theoretical maximum value for closely spaced jams with $h = h_J$ everywhere in the channel ($n_{e,max} = 0.68$ s m$^{-1/3}$) shown with solid light blue line. Modelled HEC-RAS 2D outflow including eight jams ($C_A = 50$) shown with dash dot green line.

resistance, jams were represented both as individual hydraulic structures and using a best-fit elevated resistance in HEC-RAS 2D for Penny Gill, West Cumbria, UK. The theoretical maximum resistance was used to estimate the maximum effect of closely spaced jams on outflow peak delay and attenuation.

The effect of jams increased with increasing jam-generated upstream depth relative to unobstructed water depth h_J/h_0, which increased with the dimensionless jam accumulation factor, C_A (Follett et al., 2020). A lower gap reduced outflow peak delay and relative peak reduction, with the magnitude of effect increasing with increasing gap height. The effect of jams was reduced for cases allowing overflow to the local floodplain represented by a compound channel and jam overtopping, for which the effect of jams was most pronounced at discharge levels below bankfull discharge. Identical jams placed in channels of increasing slope generate a higher relative jam-generated upstream depth and backwater volume, but lower backwater length, so that the effect of an identical jam series was most pronounced for the lowest-slope channel considered, due to higher relative backwater length.

Jams spaced more closely than $L_{bw,max}/L_s = 1$ had a decreased rate of increase in peak delay and attenuation of outflow discharge peak with increased spacing, suggesting that jam spacings much closer than $L_{bw,max}/L_s = 1$ may provide reduced value for money. The best-fit effective resistance approached the theoretical maximum value when $L_{bw,max}/L_s \geq 1$ over all inflow discharge values. For a jam with constant C_A, backwater length decreases with increasing slope, allowing closer spacing of jams in higher slope channels. Existing guidance recommending spacing of jams over a multiple of bankfull width likely partially accounts for this effect due to expected decrease in channel width with increasing slope ($B_{bf} \sim S^{-0.4}$; Parker et al., 2007). The presence of a lower vertical gap below the jam, a common engineered logjam design, prevented significant delay of flow at levels below the point of inundation of the jam lower edge, but increased the discharge value at which the jam would become overtopped, causing the jam to influence outflow discharge over a wider range of discharge values.

Software and Data Availability

The 1D network model presented in this paper has been made freely available on GitHub, titled "Leaky Barrier Advisor" (https://github.com/efollett/Leaky-Barrier-Advisor). The developer Elizabeth Follett is contactable at emf@alum.mit.edu. The year first available is 2022. Model files are written in the freely available R language with size 45 KB. R is developed for Unix-like, Windows, and Mac families and will compile and build on common Unix-like platforms. More information can be obtained from the R FAQ (Hornik and R Core Team 2022). The R language may be accessed from the Comprehensive R Archive Network (https://CRAN.R-project.org/).

The model is targeted at users estimating the effect of a series of leaky barriers on outflow discharge using sparse input data. The R language and environment was chosen for correspondence with existing hydrological models (Metcalfe et al., 2017) and to provide an open source, freely available option for previous 1D models assessing jam placement and network structure (Hankin et al. 2020).

Declaration of competing interest

The authors declare the following financial interests/personal relationships which may be considered as potential competing interests: Elizabeth Follett reports financial support was provided by the Royal Academy of Engineering's Research Fellowships programme. Elizabeth Follett reports financial support was provided by Welsh Government Sêr Cymru programme 80762-CU-241. Barry Hankin reports financial support was provided by the Natural Environment Research Council through grant NE/R004722/1. Barry Hankin reports a relationship with JBA Consulting that includes: employment.

Data availability

Link provided in the Software And Data Availability Statement of attached manuscript.

Acknowledgements

Contribution of the West Cumbria Rivers Trust and Natural Resources Wales are gratefully acknowledged. The first author has received funding from the Royal Academy of Engineering's Research Fellowships programme and the European Regional Development Fund through the Welsh Government Sêr Cymru programme 80762-CU-241. The second author has been supported by NERC grant NE/R004722/1. Thanks also to Dr Nick Chappell for supply of data, PI on the Q-NFM project for the cited NERC project code.

References

Addy, S., Wilkinson, M., 2019. Representing natural and artificial in-channel large wood in numerical hydraulic and hydrological models. WIREs Water 6, e139. https://doi.org/10.1002/wat2.1389.

Anderson, B.G., Rutherfurd, I.D., Western, A.W., 2006. An analysis of the influence of riparian vegetation on the propagation of flood waves. Environ. Model. Software 21, 1290–1296. https://doi.org/10.1016/j.envsoft.2005.04.027. Available.

Basco-Carrera, L., Warren, A., van Beek, E., Jonoski, A., Giardino, A., 2017. Collaborative modelling or participatory modelling? A framework for water resources management. Environ. Model. Software 91, 95–110. https://doi.org/10.1016/j.envsoft.2017.01.014. Available.

Bennett, S., Ghaneeziad, S., Gallisdorfer, M., Cai, D., Atkinson, J., Simon, A., Langendoen, E., 2015. Flow, turbulence and drag associated with engineered log jams in a fixed-bed experimental channel. Geomorphology 248, 172–184. https://doi.org/10.1016/j.geomorph.2015.07.046.

Beven, K., Binley, A., 1992a. The future of distributed models: model calibration and uncertainty prediction. Hydrol. Process. 6, 279–298. https://doi.org/10.1002/hyp.3360060305.

Beven, K., Binley, A., 1992b. GLUE: 20 years on. Hydrol. Process. 28, 5897–5918. https://doi.org/10.1002/hyp.10082.

Bilby, R., 1981. Role of organic debris dams in regulating the export of dissolved and particulate matter from a forested watershed. Ecology 62, 1234–1243. https://doi.org/10.2307/1937288.

Black, A., Peskett, L., MacDonald, A., Young, A., Spray, C., Ball, T., Thomas, H., Werritty, A., 2020. Natural flood management, lag time and catchment scale: results from an empirical nested catchment study. J. Flood Risk Manag., e12717 https://doi.org/10.1111/jfr3.12717.

Bouwes, N., Weber, N., Jordan, C., Saunders, W., Tattam, I., Volk, C., Wheaton, J.M., Pollock, M., 2018. Ecosystem experiment reveals benefits of natural and simulated beaver dams to a threatened population of steelhead (*Oncorhynchus mykiss*). Sci. Rep. 6, 28581 https://doi.org/10.1038/srep28581.

Burgess-Gamble, L., Ngai, R., Wilkinson, M., Nisbet, T., Pontee, N., Harvey, R., Kipling, K., Addy, S., Rose, S., Maslen, S., Jay, H., Nicholson, A., Page, T., Jonczyk, J., Quinn, P., 2018. Working with Natural Processes – Evidence Directory. Technical Report No. SC150005. Environment Agency: Horizon House, Deanery Road, Bristol, BS1 5AH.

Chow, V.T., 1959. Open-channel Hydraulics. McGraw-Hill, London, 1959.

Dadson, S.J., Hall, J.W., Murgatroyd, A., Acreman, M., Bates, P., Beven, K., Heathwaite, L., Holden, J., Holman, I.P., Lane, S.N., O'Connell, E., Penning-Rowsell, E., Reynard, N., Sear, D., Thorne, C., Wilby, R., 2017. A restatement of the natural science evidence concerning catchment-based 'natural' flood management in the UK. Proc. Royal Soc. A 473. https://doi.org/10.1098/rspa.2016.0706, 20160706.

Follett, E., Schalko, I., Nepf, H., 2020. Momentum and energy predict the backwater rise generated by a large wood jam. Geophys. Res. Lett. 47, e2020GL089346 https://doi.org/10.1029/2020GL089346.

Follett, E., Schalko, I., Nepf, H., 2021. Logjams with a lower gap: backwater rise and flow distribution beneath and through logjam predicted by two-box momentum balance. Geophys. Res. Lett. 48, e2021GL094279 https://doi.org/10.1029/2021GL094279.

Gallisdorfer, M.S., Bennett, S.J., Atkinson, J.F., Ghaneeizad, S.M., Brooks, A., Simon, A., Langendoen, E.J., 2014. Physical-scale model designs for engineered log jams in rivers. J. Hydro-environ. Res. 8, 115–128. https://doi.org/10.1016/j.jher.2013.10.002.

Geertsema, T.J., Torfs, P.J.J.F., Eekhout, J.P., Teuling, A.J., Hoitink, A.J., 2020. Wood-induced backwater effects in lowland streams. River Res. Appl. 36 (7), 1171–1182. https://doi.org/10.1002/rra.3611.

Gregory, K.J., Gurnell, A.M., Hill, C.T., 1985. The permanence of debris dams related to river channel processes. Hydrol. Sci. J. 30 (3), 371–381. https://doi.org/10.1080/02626668509491000.

Hankin, B., Hewitt, I., Sander, G., Danieli, F., Formetta, G., Kamilova, A., Kretzschmar, A., Kiradjev, K., Wong, C., Pegler, S., Lamb, R., 2020. A risk-based, network analysis of distributed in-stream leaky barriers for flood risk management. Nat. Hazards Earth Syst. Sci. 209, 256702584 https://doi.org/10.5194/nhess-2019-394.

Hankin, B., Metcalfe, P., Johnson, D., Chappell, N.A., Page, T., Craigen, I., Lamb, R., Beven, K., 2017. Flood risk management. In: (chap. Strategies for Testing the Impact of Natural Flood Risk Management Measures. InTechOpen Book Series. https://doi.org/10.5772/intechopen.68677.

Hedelin, B., Gray, S., Woehlke, S., BenDor, T.K., Singer, A., Jordan, R., Zellner, M., Giabbanelli, P., Glynn, P., Jenni, K., Jetter, A., Kolagani, N., Laursen, B., Leong, K.M., Schmitt Olabisi, L., Sterling, E., 2021. What's left before participatory modelling can fully support real-world environmental planning processes: a case study review. Environ. Model. Software 143, 105073. https://doi.org/10.1016/j.envsoft.2021.105073. Available.

Hey, R., Thorne, C., 1986. Stable channels with mobile gravel beds. J. Hydraul. Eng. 112, 671–689. https://doi.org/10.1061/(asce)0733-9429(1986)112:8(671).

Hornik, K., R Core Team, 2022. The R FAQ. Available: https://CRAN.R-project.org/doc/FAQ/R-FAQ.html.

Ismail, H., Xu, Y., Liu, X., 2021. Flow and scour around idealized porous engineered log jam structures. J. Hydraul. Eng. 147, 04020089 https://doi.org/10.1061/(ASCE)HY.1943-7900.0001833.

Julien, P.Y., 1998. Erosion and Sedimentation, first ed. Cambridge University Press, Cambridge.

Julien, P.Y., 2010. Erosion and Sedimentation, second ed. Cambridge University Press, Cambridge.

Keller, E., Swanson, F., 1979. Effects of large organic material on channel form and fluvial processes. Earth Surf. Process. Landforms 4, 361–380. https://doi.org/10.1002/esp.3290040406.

Kjeldsen, T.R., Stewart, E.J., Packman, J.C., Folwell, S.S., Bayliss, A.C., 2005. Revitalisation of the FSR/FEH Rainfall-Runoff Method. Defra R&D Technical Report FD1913/TR.

Leakey, S., Hewett, C., Glenis, V., Quinn, P., 2020. Modelling the impact of leaky barriers with a 1D Godunov-type scheme for the shallow water equations. Water 12, 371. https://doi.org/10.3390/w12020371.

Lewis, E., Birkinshaw, S., Kilsby, C., Fowler, H.J., 2018. Development of a system for automated setup of a physically based, spatially distributed hydrological model for catchments in Great Britain. Environ. Model. Software 108, 102–110. https://doi.org/10.1016/j.envsoft.2018.07.006. Available.

Linstead, C., Gurnell, A.M., 1999. Large Woody Debris in British Headwater Rivers: Physical Habitat Role and Management Guidelines. Environment Agency R & D Technical Report W185. Available: https://assets.publishing.service.gov.uk/government/uploads/system/uploads/attachment_data/file/290559/str-w185-e-e.pdf.

Malcherek, A., 2018. Eine neue, auf der impulsbilanz basierende theorie zur hydraulik des schützes – ein diskussionsbeitrag. Wasserwirtschaft 5, 40–69. https://doi.org/10.1007/s35147-018-0215-8.

Metcalfe, P., Beven, K., Hankin, B., Lamb, R., 2017. A modelling framework for evaluation of the hydrological impacts of nature-based approaches to flood risk management, with application to in-channel interventions across a 29-km^2 scale catchment in the United Kingdom. Hydrol. Process. 31, 1734–1748.

Parker, G., Wilcock, P., Paola, C., Dietrich, W., Pitlick, J., 2007. Physical basis for quasi-universal relations describing bankfull hydraulic geometry of single-thread gravel bed rivers. J. Geophys. Res. 112, F04005 https://doi.org/10.1029/2006JF000549.

Persi, E., Petaccia, G., Sibilla, S., Lucia, A., Andreoli, A., Comiti, F., 2019. Numerical modelling of uncongested wood transport in the Rienz River. Environ. Fluid Mech. 20, 539–558. https://doi.org/10.1007/s10652-019-09707-8.

Ruíz Villanueva, V., Castellet, E., Diez-Herrero, A., Bodoque, J., Sanchez-Juny, M., 2014. Two-dimensional modelling of large wood transport during flash floods. Earth Surf. Process. Landforms 39, 438–449. https://doi.org/10.1002/esp.3456.

Senior, J.G., Trigg, M.A., Willis, T., 2022. Physical representation of hillslope leaky barriers in 2D models: a case study from the Calder Valley. J. Flood Risk Manag. 15 (3), e12821.

Schalko, I., Schmocker, L., Weitbrecht, V., Boes, R., 2018. Backwater rise due to large wood accumulations. J. Hydraul. Eng. 144, 04018056 https://doi.org/10.1061/(ASCE)HY.1943-7900.0001501.

Voinov, A., Bousquet, F., 2010. Modelling with stakeholders. Environ. Model. Software 25, 1268–1281. https://doi.org/10.1016/j.envsoft.2010.03.007. Available.

Voinov, A., Kolagani, N., McCall, M.K., Glynn, P.D., Kragt, M.E., Ostermann, F.O., Pierce, S.A., Ramu, P., 2016. Modelling with stakeholders—next generation. Environ. Model. Software 77, 196–220. https://doi.org/10.1016/j.envsoft.2015.11.016. Available.

Wohl, E., Angermeier, P.L., Bledsoe, B., Kondolf, G.M., MacDonnell, L., Merritt, D.M., Palmer, M.A., Poff, N.L., Tarboton, D., 2005. River restoration. Water Resour. Res. 41, W10301 https://doi.org/10.1029/2005WR003985.

Wohl, E., Bledsoe, B., Fausch, K., Kramer, N., Bestgen, K., Gooseff, M., 2016. Management of large wood in streams: an overview and proposed framework for hazard evaluation. J. Am. Water Resour. Assoc. 52, 315–335. https://doi.org/10.1111/17521688.12388.

Wohl, E., Jaeger, K., 2009. A conceptual model for the longitudinal distribution of wood in mountain streams. Earth Surf. Process. Landforms 34, 329–344. https://doi.org/10.1002/esp.1722.

Wren, E., Barnes, M., Janes, M., Kitchen, A., Nutt, N., Patterson, C., Piggott, M., Robins, J., Ross, M., Simons, C., Taylor, M., Timbrell, S., Turner, D., Down, P., 2022. The Natural Flood Management Manual. C802. CIRIA, London, UK.

Yorkshire Dales Rivers Trust, 2021. Naturally resilient: leaky dams. Available: https://www.ydrt.org.uk/wp-content/uploads/2021/04/NFM-Leaky-Dams-guide.pdf.

Yochum, S.E., Comiti, F., Wohl, E., David, G.C.L., Mao, L., 2014. Photographic Guidance for Selecting Flow Resistance Coefficients in High Gradient Channels. General Technical Report No. RMRS-GTR-323. United States Forest Service Rocky Mountain Research Station. Available: https://www.fs.usda.gov/treesearch/pubs/46250.